Visualization of Energy Flow in Wireless Power Transfer Systems

Hanwei Wang
Department of Physics
Tsinghua University
Beijing, China
wanghw15@mails.tsinghua.edu.cn

Cheng Zhang
School of Electrical and Electronic
Engineering
University of Manchester
Manchester, United Kingdom
cheng.zhang@manchester.ac.uk

Shu Yuan Ron Hui
Department of Electrical can Electronic
Engineering
University of Hong Kong
Hong Kong SAR, China
ronhui@eee.hku.hk

Abstract—**A time-efficient computational framework to plot the time-varying and time-averaged space distribution of Poynting vectors in an inductive wireless power transfer system is presented in this paper. It can deal with any arbitrarily shaped winding. The time and space complexities are reduced compared to popular CEM methods. This framework uses 1-dimensional segmentation instead of 3-dimensional mesh gridding. The currents in the windings are solved analytically and the field strength values are directly calculated by numerical integrations. Several examples are included in this paper. It can be further integrated with design and optimization tools for wireless power transfer applications that would allow automated circuit design. It can also help industrial designers understand the energy flow in air intuitively.**

Keywords—visualization, wireless power transfer, Poynting vector, calculation method

I. INTRODUCTION

Inductive coupling wireless power transfer has been applied in various daily-life consumer products for years, bringing us great convenience. It can make electric appliances completely water-resistant, e.g. the toothbrushes and the action cameras; it can also save people's efforts of connecting the charging cables, e.g. the wireless charging for smartphones.[1-2] Some recent works show that a decent amount of power can be transmitted to an arbitrarily placed load within the certain region [3-6], and commercialized products are ready for the market. [7]

When designing the WPT applications, often the most concerned parameters are the amount of power transmitted and the energy efficiency of the system.[8] It is, however, difficult to understand intuitively how energy is being transmitted through the air. In [9], the time-varying magnetic fields around the coils are plotted using ANSYS Maxwell, a popular commercial computational electromagnetics (CEM) software. The animations can show the movement of energy "bubbles". But it doesn't show the actual energy flow among coils, neither does it justify the direction of energy flow. In order to see the energy flux emitting from the transmitter coils and terminating in the receiver coils, the best way to represent the energy flow should be by using Poynting vectors.

In this paper, a time-efficient and light-weight computation framework to visualize the time-varying and time-averaged Poynting vectors (as well as other field quantities) in an inductive WPT system is proposed. Windings are not limited to regular shapes, and the calculation complexity (in both time and space) is much smaller than traditional 3D CEM algorithms when it comes to visualization. This method can be implemented by a variety of programming languages and is possible to be integrated for further automated design and optimization purposes. It is also a tool that can be useful for industrial designers to have an intuitive understanding of the energy path in the air when designing the cases of the products.

The result shows the continuous time-averaged energy flux from the source winding to the load winding. It also shows that the time-varying apparent energy flux oscillates and the peak values are bigger than the time-averaged values.

II. METHODOLOGY

Magnetoquasistatic analysis is used in this framework as the operating frequency of inductive WPT applications are relatively low (below 200MHz) compared to the physical sizes of the winding structures (several centimeters to meters). The wave propagation delay is ignored. The definition of the Poynting vector used in this work is $\mathbf{S} = \mathbf{E} \times \mathbf{H}$. The proposed method consists of six steps. Each step can be regarded as an atomic operation and can be implemented independently.

A. Describe the spatial trajectory of the windings

It is assumed that there are n windings in a wireless power transfer system: $l_1, l_2, \cdots, l_n$. For each winding l_i, it is divided into m segments $dl_1, dl_2, \cdots, dl_m$. The minimal length of each segment is recommended to be exactly the diameter of the wire used. This will make sure that all physically feasible windings can be accurately modeled while keeping a relatively low number of segment counts. In practical implementations, each segmented cell contains information of the starting and the ending vectors relative to the spatial reference point.

B. Obtain basic circuit parameters

Each winding in a WPT system is supposed to be connected with external compensation capacitors to form a resonator. Practically the winding also has its parasitic resistance and capacitance. X_n is the total series reactance of resonator circuit n and R_n is the total equivalent series resistance. The transmitter circuits are connected to voltage or current sources and the receiver circuits are connected to loads.

The mutual and self-inductance values are determined by the physical dimensions and positions of the winding, unlike other values which are appointed externally. The inductance values can be calculated from the vectors of winding segments using Neumann formula [10].

$$M_{ij} = \frac{\mu_0}{4\pi} \oint_{l_i} \oint_{l_j} \frac{\mathrm{d}\boldsymbol{l_i} \cdot \mathrm{d}\boldsymbol{l_j}}{\left| \boldsymbol{r}_{\mathrm{d}l_i} - \boldsymbol{r}_{\mathrm{d}l_j} \right|} \tag{1}$$

where l_i and l_j are contours of two windings, $\mathrm{d}\boldsymbol{l_i}$ and $\mathrm{d}\boldsymbol{l_j}$ are infinitesimal segment vectors on the two windings and $\boldsymbol{r}$ vectors are the displacement vectors refer to the reference origin. In the case that $i = j$, M_{ij} becomes the self-inductance of the winding and the integral term cannot be computed if $\mathrm{d}\boldsymbol{l_i}$ and $\mathrm{d}\boldsymbol{l_j}$ are the same segment. An alternative closed-form formula is used to replace the integral term. For wires with a circular cross-section, the following formula can be used. [11]

$$L_{part} = \frac{\mu_0}{2\pi} \left[l \log\left(\frac{l + \sqrt{l^2 + \rho^2}}{\rho} \right) - \sqrt{l^2 + \rho^2} + \frac{l}{4} + \rho \right] \tag{2}$$

where l is the length of the segment and ρ is the radius of the cross-section. It is verified by experiments that when the length of the segment is equal to the diameter of the wire, the calculated self-inductance is at its most accuracy to predict the measurement value.

C. Calculate the current amplitudes and phases for all the windings

The ac currents in each winding directly contribute to the electric and magnetic fields in space and they can be calculated using (3).

$$\begin{bmatrix} R_1 + jX_1 & j\omega M_{12} & j\omega M_{13} & \cdots & j\omega M_{1n} \\ j\omega M_{12} & R_2 + jX_2 & j\omega M_{23} & \cdots & j\omega M_{2n} \\ j\omega M_{13} & j\omega M_{23} & R_3 + jX_3 & \cdots & j\omega M_{3n} \\ \vdots & \vdots & \vdots & \ddots & \vdots \\ j\omega M_{1n} & j\omega M_{2n} & j\omega M_{3n} & \cdots & R_n + jX_n \end{bmatrix} \begin{bmatrix} I_1 \\ I_2 \\ I_3 \\ \vdots \\ I_n \end{bmatrix} = \begin{bmatrix} V_1 \\ V_2 \\ V_3 \\ \vdots \\ V_n \end{bmatrix} \tag{3}$$

where R and X have been defined in subsection B, M_{ij} is the mutual inductance between the windings of circuit i and j, I_i is the current in the winding i and V_i is the external source voltage for circuit i. For non-transmitter circuits, the voltage is always 0.

The current values solved from (3) are complex numbers that contain information of magnitudes and phases. To calculate the time-varying fields, instantaneous current values regarding different phase angles are calculated from the expansion of these complex numbers. To calculate the time-averaged fields, the currents are directly substituted in equations and the real part of the power (Poynting vector) is taken.

D. Generate the observation points

A region of interest (ROI) is defined. Usually, it is in $\Re^3$ space so that the trajectory of the windings can be properly displayed. A set of observation points are sampled within ROI. Depending on the form of presentation or demand of usage, these points may be sampled in $\Re^3$, $\Re^2$, or $\Re^1$ space. For example, in this paper where only 2D projections can be printed, observation points are sampled in a representative plane (the plane in the center), and the viewing direction is perpendicular to the plane.

It does not matter if the ROI covers all the windings in the system or not because this framework only calculates field values at observation points, instead of computing all the cells in the entire ROI like traditional CEM methods.

E. Calculate $\boldsymbol{H}$, $\boldsymbol{E}$, $\boldsymbol{S}$ fields for each observation point

H field at the point is calculated from Biot-Savart Law:

$$\boldsymbol{H} = \sum_{i=1}^{n} \oint_{l_i} \frac{I_i \mathrm{d}\boldsymbol{l_i} \times \boldsymbol{r}_{\mathrm{d}l_i}}{4\pi \left| \boldsymbol{r}_{\mathrm{d}l_i} \right|^3} \tag{4}$$

where $\boldsymbol{r}_{\mathrm{d}l_i}$ is the displacement vector from $\mathrm{d}\boldsymbol{l_i}$ to the point of observation.

E field at the point is calculated from the time derivative of the magnetic vector potential:

$$\boldsymbol{A} = \sum_{i=1}^{n} \oint_{l_i} \frac{\mu_0 I_i}{4\pi} \mathrm{d}\boldsymbol{l_i} \tag{5}$$

$$\boldsymbol{E} = -\frac{\partial \boldsymbol{A}}{\partial t} = -j\omega \boldsymbol{A} \tag{6}$$

Then finally the Poynting vector is calculated:

$$\boldsymbol{S} = \boldsymbol{E} \times \boldsymbol{H} \tag{7}$$

F. Plot the vectors together with the winding traces

The last step is to plot the windings and visualize the Poynting vectors appropriately. A variety of plotting libraries can be used. In this work, *gnuplot* is used and Poynting vectors are simply plotted from the observation points with rescaled arrows representing both the direction and the strength.

III. Performance Evaluation

The computing time generally determines the usage and usability of the calculation framework. It is acceptable to spend hours rendering a single frame just for artistic presentation, but if each run only takes several seconds, it would be possible to be used as assessment functions for automated optimizations.

The time and space complexities of the unoptimized algorithms for each step in the previous section are analyzed in Table I.

TABLE I.   TIME AND SPACE COMPLEXITIES OF EACH STEP

Step	Time Complexity	Space Complexity	Remarks
A	$O(n \times m)$ $\approx O(m)$	$O(n \times m)$ $\approx O(m)$	n: number of windings, usually a small number
B	$O\left(\frac{n(n-1)}{2} \times m^2 \right)$ $\approx O(m^2)$	$O(n \times m)$ $\approx O(m)$	m: number of segments, usually a large number

TABLE I CONTINUED

C	$O(n^3)$	$O(n^2)$	As n is small, these are almost $O(1)$
D	$O(k)$	$O(k)$	k: number of points
E	$O(n \times m \times k)$ $\approx O(m \times k)$	$O(n \times m + k)$ $\approx O(m)$	Ignoring small numbers
F	$O(k)$	$O(k)$	Depending on library

Intuitively compared to traditional CEM algorithms whose both time and space complexities are $O(n_c^3)$ (where n_c is cells/segments per dimension)[12], the heaviest load in the proposed framework is only about $O(m^2)$ in time and $O(m)$ in space (where m is segments per winding, and considering that the number of circuits n is a small number). Also, this method only takes one pass to get the final values whereas some CEM algorithms take several passes to converge. This method has advantages over commercial CEM software in some aspects. However, it is not supposed to directly compete with commercial software as the modeling mechanism is so different. Both of two approaches are able to deal with arbitrary coils. This method treats conductors as line trajectories instead of 3D blocks and it only solves for fields at concerned observation points instead of the entire field.

As an example, a system (the straight domino case in the next section) with $n = 8$, $m = 6911$, $k = 1600$ costs less than 7MB in memory consumption and about 8 min to generate 36 frames using an unoptimized single-thread C++ program running on a 2014 desktop computer (i7-4790K 4GHz, CPU utilization rate<20%, compiled by *mingw-g++*).
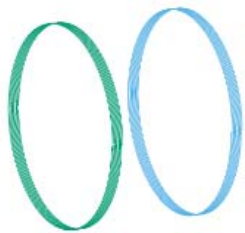
IV. RESULT

A. Two-Coil System

Fig. 1. A Two-Coil Wireless Power Transfer System (2D projection from a 3D plot).

This is one of the simplest WPT systems. Two identical coils are aligned coaxially and the distance between them is 20cm. Each coil has a diameter of 30cm and consists of 11 turns of 1.5mm diameter Litz wire, contributing to a width of 2cm, as shown in Fig. 1. Both the transmitter (green) and receiver (blue) coils are compensated with 1nF capacitors in series. Each circuit has a serial resistance of 0.75Ω and the load impedance is 10Ω. The transmitter is driven by a 553kHz voltage source with the amplitude of 10V and a reference phase angle of 0. The calculated current in the transmitter is $0.2746\angle - 0.1042$ A, the receiver current is $0.4988\angle - 1.523$ A. The Poynting vectors in the plots are scaled with a constant factor for best visual effect and the absolute amplitudes of the voltages and currents are less important.

Fig. 2 shows the time-varying Poynting vector fields for every 10-degree phase angle. Only the first half cycle is shown here and the second half is a repeat. The two coils are coaxial on the x-axis and the observation points are uniformly sampled from yz-plane so that the cross-sectional view of the field is plotted.
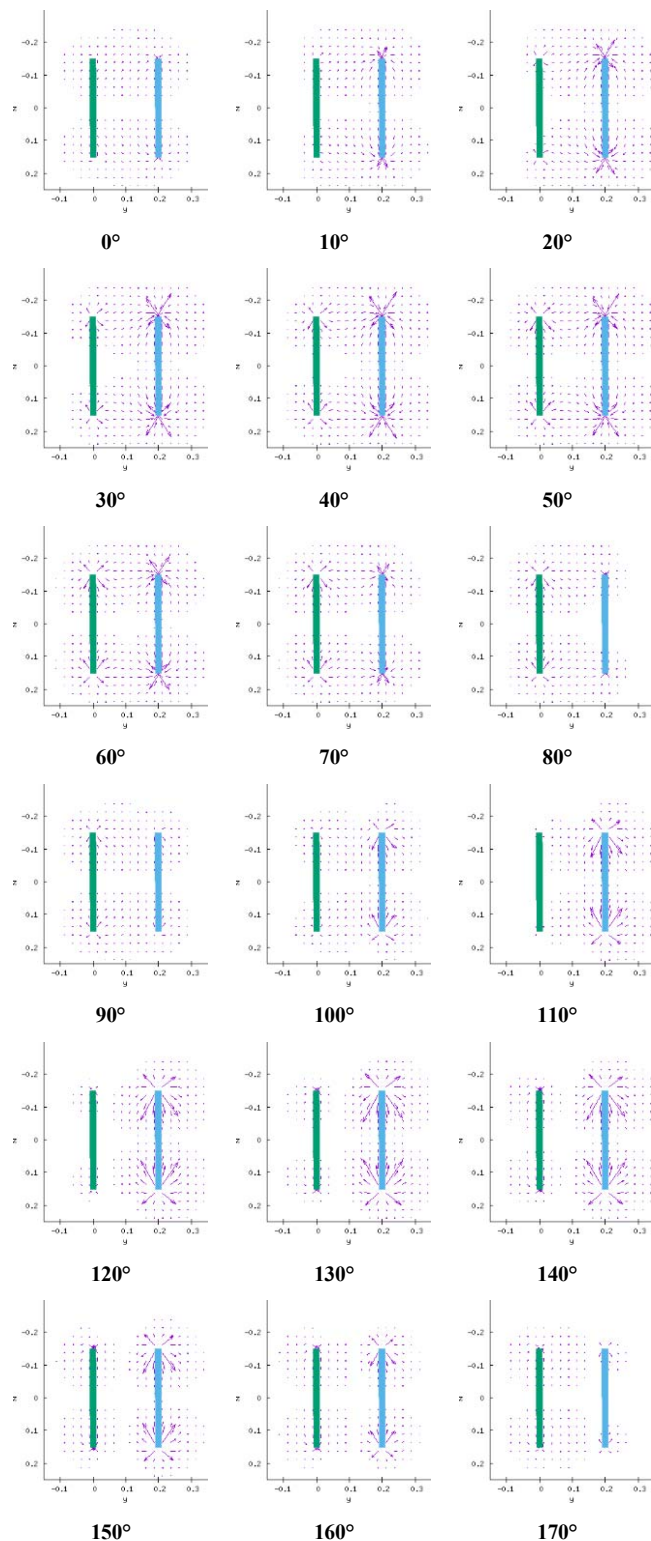

Fig. 2. Time varying Poynting vector field of a two-coil WPT system.

It can be seen from the animated plots that the apparent power "flux" firstly flows from the transmitter winding to the receiver winding, then flips the direction, and oscillating at twice the operating frequency. (The arrows around the blue coil look like leaving the coil for plots of 10°~70°. These are "overshoot". They have longer vector length but still pointing towards the blue coil.) The "flux" leaves or enters the winding from all directions instead of towards the opponent only. It is also noticed that the energy strength is unevenly distributed, for places around the transmitting coil have weaker energy level than those around the receiving coil. This only shows there is bidirectional energy flow between the two coils but does not tell why and how energy is transferred. Both coils are releasing and absorbing energy repetitively.
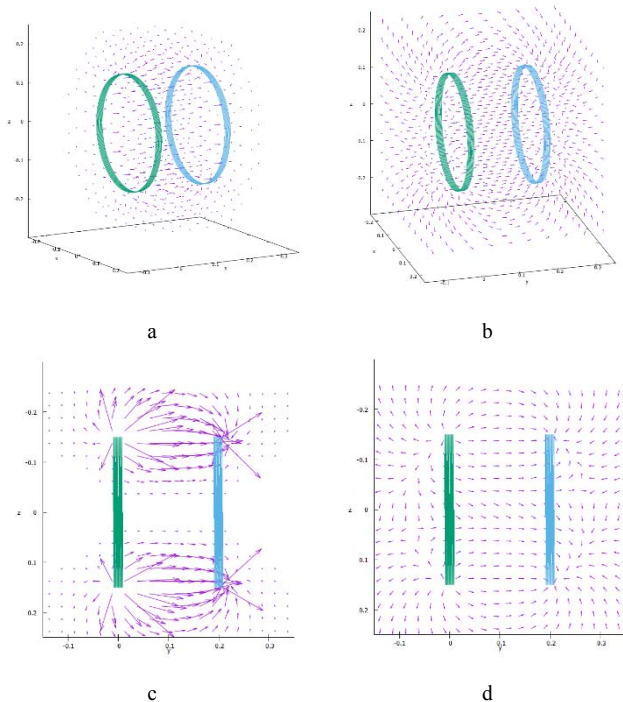
Fig. 3. Time-averaged Poynting vectors for a two-coil WPT system.

The time-averaged plots show that energy is exiting from the green winding and enters the blue winding, and the amount is balanced, as shown in Fig. 3. The lengths of vectors in Fig. 3a and Fig. 3c are proportional to the strength of the Poynting vectors, and in Fig. 3b and Fig. 3d they are normalized so that the pattern is easier to see (also avoids "overshoot"). The 3D plots are unclear on plane printed medium; however, they look good when viewing on monitors with the interactive movement of POV (rotations).

B. Eight-Coil Straight domino system

This example shows an eight-coil straight domino system that appeared in [9, 13]. The left-most coil is the transmitter and the rightmost coil is the receiver. Fig. 4 shows the scaled time-averaged Poynting vectors and Fig. 5 shows the normalized vectors on yz-plane. The energy flux formed a straight rigatoni-shaped beam from the transmitter to the receiver. Though the current magnitudes on each coil vary a lot, the averaged energy flow looks uniform and straight.
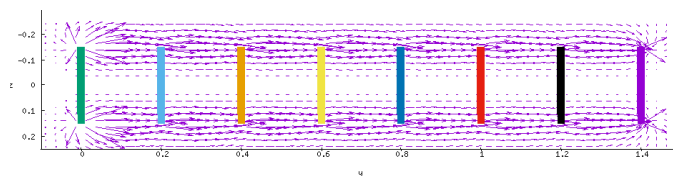

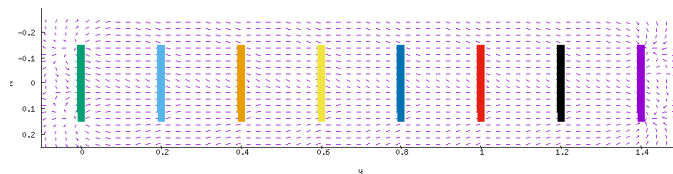Fig. 4. Time-averaged Poynting vectors for an eight-coil straight domino system with proportional lengths.

Fig. 5. Time-averaged normalized Poynting vectors for an eight-coil straight domino system.

C. Circular Domino System

This example shows a system with eight coils placed in a ring form, with the left-most coil is connected with a voltage source and one of the coils is connected with a resistive load. Similar structures can be found in [9,14]
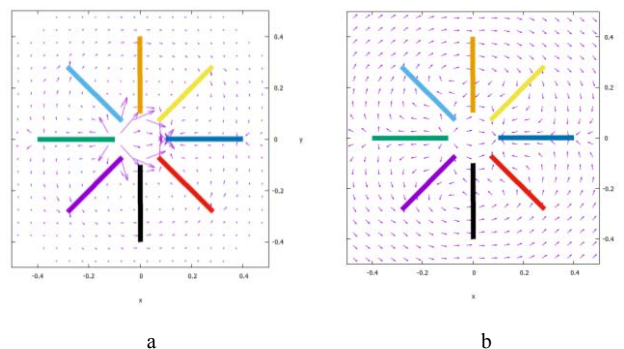

Fig. 6. Time-averaged Poynting vectors for an eight-coil circular domino system in even mode.

Fig. 6 shows the energy flow in even mode where the load is placed at the symmetric position, right-most in the picture. The energy flow is also symmetric, following two paths ways.
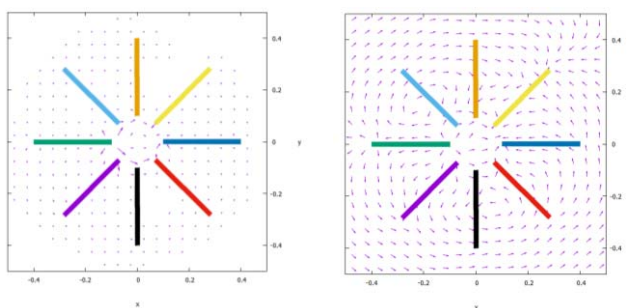

Fig. 7. Time-averaged Poynting vectors for an eight-coil circular domino system in odd mode.

Fig. 7 shows the case where the resistive load is connected to the light-yellow coil in the first quadrant and the system is in

odd mode. The energy flow can still be clearly seen exiting from the source and entering the load.

It is also noticed that in a circular domino WPT system the energy flow is denser in the inner edge.

D. Ball-Joint WPT System

In [15] two hemispherical coils are embedded in a ball joint structure to enable energy transferred over the joint wirelessly. This example is to show that the framework can handle all kinds of windings. The outer coil in green is the transmitter and the inner blue coil is the receiver.
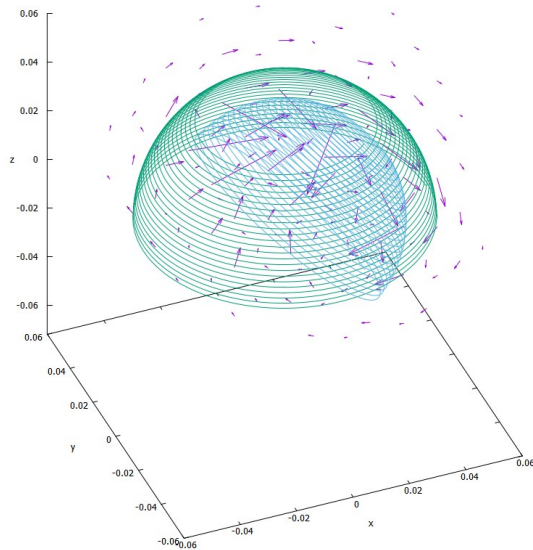

Fig. 8. Time-averaged Poynting vectors for a ball-joint WPT system in 3D.
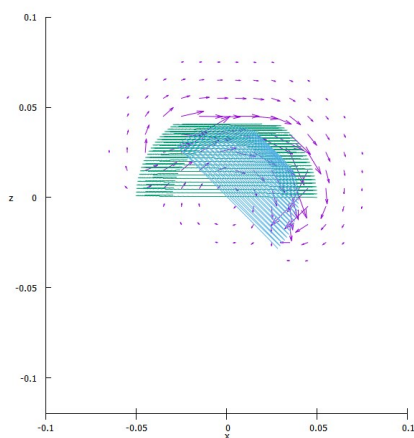

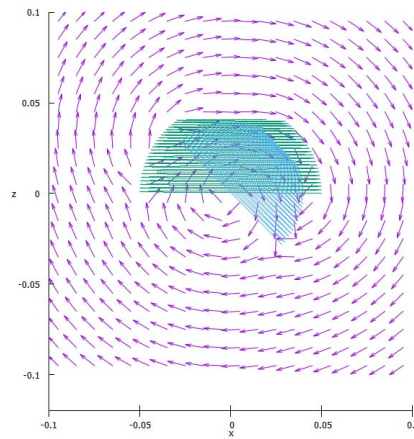Fig. 9. Time-averaged Poynting vectors for a ball-joint WPT system with proportional vectors on xz-plane.

Fig. 10. Time-averaged Poynting vectors for a ball-joint WPT system with normalized vectors on xz-plane.

When plotting the energy flow in a WPT system, the only directly related parameters are the magnitudes and phases of the currents in each winding. It is interesting to find these current values do contain the information of spatial energy flow, which is not obvious but makes perfect sense in theory.

V. CONCLUSION

In conclusion, this paper presents a time-efficient way to plot the Poynting vector fields in an inductive WPT system. It can be applied to arbitrary irregular windings. Due to low calculation complexity, it can be potentially integrated with automated design and optimization processes. The produced plots show the spatial distribution of energy flow from the source windings to the load windings. It is also noticed that the time-varying oscillating apparent energy flux has a much higher amplitude.

ACKNOWLEDGEMENT

REFERENCES

[1] Wireless Power Consortium, "The Qi Wireless Power Transfer System Power Class 0 Specification: Parts 1 and 2: Interface Definitions," ver 1.2.2; Apr 2016.

[2] Tim Bradshaw, "Review: the joys of smartphone wireless chargers," Financial Times, https://www.ft.com/content/871843e8-aa78-11e7-93c5-648314d2c72c, accessed on Feb 6, 2019

[3] P. Sun, Y. Dong, H. Ye and H. Zhao, "A Wireless Power Transfer CPS Based on 2D Omni-directional Rotating Magnetic Field," 2016 IEEE International Conference on Software Quality, Reliability and Security Companion (QRS-C), Vienna, 2016, pp. 252-258.

[4] M. Sasaki and M. Yamamoto, "Exciting voltage control for transfer efficiency maximization for multiple wireless power transfer systems," 2017 IEEE Energy Conversion Congress and Exposition (ECCE), Cincinnati, OH, 2017, pp. 5523-5528.

[5] W. M. Ng, C. Zhang, D. Lin, and S. Y. R., Hui "Two-dimensional and three-dimensional omnidirectional wireless power transmission," IEEE Trans. Power Electron., vol. 29, no. 9, pp. 4470–4474, Sep. 2014.

[6] L. Shi, Z. Kabelac, D. Katabi, and D. J. Perreault, "Wireless Power Hotspot that Charges All of Your Devices," Proceedings of the 21st Annual International Conference on Mobile Computing and Networking (MobiCom '15). ACM, New York, NY, USA, 2-13.

[7] Pi Inc., "Pi Debuts the World's First Contactless, Wireless Charger for Consumer Devices," Pi Press Release, https://static1.squarespace.com/static/598d0d4f6a49637f69cdd3b0/t/59c058fcb1ffb6a20b118740/1505777917235/Pi+Press+Release.pdf, accessed on Feb 6, 2019

[8] S. Y. Ron Hui, W. Zhong, and C. K. Lee, "A critical review of recent progress of mid-range wireless power transfer," IEEE Transactions on Power Electronics, vol. 29, no. 9, pp. 4500-4511, Sept 2014.

[9] C. Zhang, W. Zhong, X. Liu, and S. Y. R. Hui, "A Fast Method for Generating Time-Varying Magnetic Field Patterns of Mid-Range Wireless Power Transfer Systems," IEEE Transactions on Power Electronics, vol. 30, no. 3, March 2015.

[10] A. E. Ruehli, "Equivalent Circuit Models for Three-Dimensional Multiconductor Systems," IEEE Transactions on Microwave Theory and Techniques, vol. MTT-22, pp. 216-221, 1974.

[11] E. B. Rosa and L. Cohen, "Formulae and Tables for the Calculation of Mutual and Self-inductance," Bulletin of the Bureau of Standards, vol. 5, pp. 35-50, 1907.

[12] D. B. Davidson, "A Review of Important Recent Developments in Full-wave CEM for RF and Microwave Engineering," 2004 3rd International Conference on Computational Electromagnetics and Its Applications Proceedings, 2014.

[13] W. X. Zhong, "An Investigation into the Use of Coil-Resonators in Domino Forms for Wireless Power Transfer," Doctor of Philosophy, Department of Electronic Engineering, City University of Hong Kong, Hong Kong, 2012.

[14] W. X. Zhong, L. Chi Kwan, and S. Y. R. Hui, "Wireless Power Domino-Resonator Systems With Noncoaxial Axes and Circular Structures," Power Electronics, IEEE Transactions on, vol. 27, pp. 4750-4762, 2012.

[15] C. Zhang, D. Lin, and S. Y. R. Hui, "Ball-Joint Wireless Power Transfer Systems," Power Electronics, IEEE Transactions on, vol. 33, pp. 65-72, 2018.